E JOURNAL

Green Part Properties as Design Driver for “First Time Right” within sinter-based Additive Manufacturing introduced on the examples of Cold Metal Fusion and Metal FFF

David Stachg (M.Sc.) [a], Tim Marter (M.Sc.) [b], Prof. Dr.-Ing. Jens Telgkamp [a]

[a] Hamburg University of Applied Sciences Berliner Tor 21, 20099 Hamburg, Germany

[b] Element22 GmbH Wischhofstraße 1-3, 24148 Kiel, Germany

https://doi.org/10.58134/fh-aachen-rte_2025_002

Zusammenfassung In diesem Artikel werden Merkmale von Bauteilen untersucht, die mit den Verfahren Cold Metal Fusion (CMF) und Metal Fused Filament Fabrication (MFFF) hergestellt werden. Beide Prozesse sind Verfahren der sinterbasierten Additiven Fertigung (SBAM). Die Ergebnisse der durchgeführten Untersuchungen sind ein Beitrag zur Bauteilgestaltung im Sinne des „First Time Right“. Die durch das Eigengewicht der Bauteile induzierten Spannungen werden analysiert und als Konstruktionsfaktor interpretiert. Die Unterschiede im Versagensverhalten von Bauteilen beider Technologien werden aufgezeigt und im Zusammenhang mit der Bauteilgestaltung diskutiert. Neben der Möglichkeit, konventionell ausgelegte SBAM-Bauteile zu bewerten, zeigen die Ergebnisse auch Potenziale für die automatisierte Bauteilgestaltung auf. Es wird ein Lastfall zur Auslegung von Bauteilen erarbeitet, der die Anforderungen des Entbinderns und Sinterns berücksichtigt. Die Erkenntnisse werden in einer Fallstudie umgesetzt, in der ein bestehendes Bauteil mittels Topologieoptimierung ein Redesign erhält.

Abstract This paper examines features of parts manufactured via the processes cold metal fusion (CMF) and metal fused filament fabrication (MFFF), which are both categorized as sinter-based additive manufacturing (SBAM) processes. The results of the investigations are a step towards part design for “First Time Right”. Stresses induced by parts’ dead load are analyzed and interpreted as a design driver. The differences in the failure behavior of parts from both technologies are shown and discussed in the context of part design. In addition to the possibility of evaluating conventionally designed SBAM parts, the findings also show potential for automated part design. A load case is established to design parts suitable for debinding and sintering. The findings are implemented in a case study in which an existing part is receiving a redesign via topology-optimization.

Introduction and motivation

The industrialization of additive manufacturing (AM) is increasing steadily. The processing of metals is of particular importance for the manufacturing of mechanically loaded components. For established powder-based processes, mainly laser powder bed fusion (LPBF), the high costs still represent an obstacle to series application. However, recently the focus of investigations has turned increasingly to processes that do not directly process the final material. Within these multiple-step processes [1], the first step consists of the processing of polymer-metal combinations, also referred to as feedstocks, via AM. Thus, so-called green parts are generated. In follow-up processes, the polymer is expelled and the final material properties are established. These processes are carried out analogously to the subsequent processing of green parts produced by metal injection molding (MIM). Based on the necessary processes contained, these multiple-step processes are also called sinter-based AM (SBAM) processes.

Sinter-based process routes have economic and ecological potential, especially compared to more established metallic AM-processes [2,3]. The necessary subsequent steps influence the cost structure. Due to the shrinkage that occurs and the potential for distortion or even collapse, the direct manufacturing for batch size 1 is still a challenge. The increasing realization of “First Time Right” through enhanced simulations and further knowledge gain will have a positive effect on this cost structure [4]. In addition, the post processing steps create additional requirements for part design. Parts consistently experience shrinkage, and their design will decide about success or distortion respectively collapse taking place during the manufacturing process. The aspect of anisotropic shrinkage, which can lead to undesired deformation, is examined in recent studies such as [5] for SBAM or [6] for sintering in general.

The aspect of collapsing of structural features is addressed in this paper. The focus of this paper lies on the SBAM processes cold metal fusion (CMF) and metal fused filament fabrication (MFFF).

General processes

Within SBAM processes, a so-called feedstock is processed. This feedstock consists of a metallic alloy, which is mixed and homogenized with different polymers, so-called binders. The binders fulfil various tasks during the manufacturing process: Enabling plasticization of the feedstock and thus enabling to process the feedstock with polymer AM technologies (main binder), ensuring cohesion of the metal particles after removal of the main binder (backbone), enabling the best possible interaction between the metal particles and the other binders (additive).

After printing, the parts consist of the feedstock, i.e. the metal-polymer compound. The parts in this stage are called green parts. These green parts then undergo chemical debinding, during which the main binder is removed. This is done using a chemical solvent. The next step is thermal debinding and subsequent sintering. This takes place in a furnace at temperatures below the melting temperature of the metal alloy. This process step takes place in a vacuum or in a protective gas atmosphere. After debinding, the parts are called brown parts. Green parts are fragile, brown parts even more so. They may only be exposed to low loads. Throughout the described process chain, the components experience typically shrinkage of 10-20 %, depending on the processes and material composition.

Following the logic of [7], the technologies CMF and MFFF belong to the indirect metal AM processes. The printed products must be post-processed by the application of energy so that they not only possess the required geometry but also the necessary material properties. This energy contribution takes place within the sintering process.

In the CMF process, the green part is printed via selective laser sintering (SLS). The feedstock is provided as a powder. The main binder is melted layer by layer. Compared to other metallic powder bed processes, less energy is required and the resulting residual stresses are of a different order of magnitude [8,9]. In addition, the process requires hardly any support structures that are in direct contact with the component. The parts must be depowdered before the chemical debinding. Due to the fragile state of the parts, the depowdering can be critical and should be considered within the part design. This limits the potential resolution of the SLS process. Experience has shown that the shrinkage of the parts during the process is homogeneous in all spatial directions and amounts to 14 %. The procedure of the CMF process is illustrated in Figure 1.

Within the MFFF process, feedstock is processed in filament format. The filament is heated, plasticized and extruded through a nozzle to generate the part layer by layer. Depending on the part geometry, support structures are inevitable. MFFF parts experience anisotropic shrinkage during the process depending on the material and process parameters, as described for instance in [10].

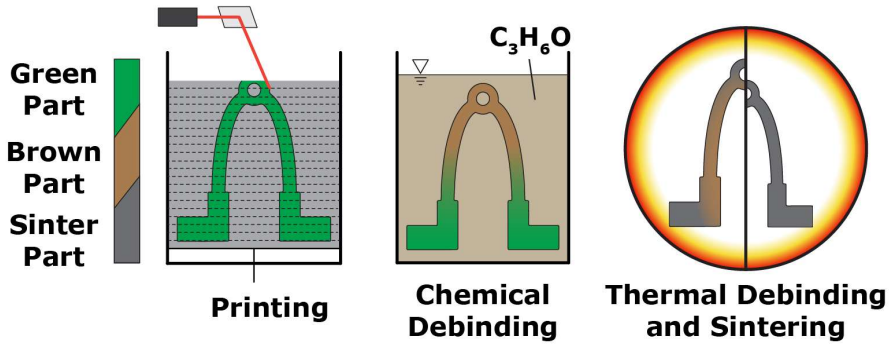

Figure 1: Main process steps within CMF

Due to the multiple-step character of the SBAM processes, part design requirements from different domains must be considered. For green part manufacturing, the design guidelines for SLS and FFF as listed for instance in [11] are applicable to the technologies discussed in this paper. The necessary processing steps of debinding and sintering result in further requirements for the design as discussed in [12]. Design principles in the context of SBAM, which are of a qualitative nature and can be found e.g. in [13]. There are investigations on design rules, i.e. qualitative guidelines, in this context as for example in [14].

Determination of green part properties and resulting design rules

The numerous design rules for polymer-based AM provide guidance on the design of parts. Depending on the aspect, specific values are given for specific geometric elements (e.g. in [15,16]). The application of such design rules poses challenges both in manual part design as well as in automated design [17]. However, these rules also enable a systematic evaluation of part designs with respect to their manufacturability via AM processes.

The limits of manufacturability of polymer AM must not be exceeded. A manufacturable green part is a mandatory, but not sufficient prerequisite for a manufacturable sinter part. Design rules from this field are therefore a mandatory requirement for SBAM. The intersection of polymer AM-compatible design and sinter-compatible design is the suitable design for SBAM (see figure 2).

It seems that the requirements of the debinding and sintering process rather limit the possibilities of manufacturability for SBAM parts. Internal stresses are a probable root cause for part collapse. One cause of these internal stresses is the dead load of a part. With established direct AM processes, dead load of parts does not pose a risk. This is different in the context of SBAM. The tensile strengths of green parts are in the single-digit MPa or three-digit kPa range [18,19], and even lower values can be assumed for brown parts.

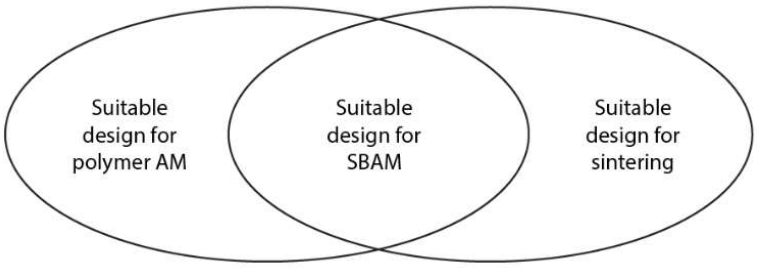

Figure 2: Relationship between domain-specific design requirements

In the following, it is discussed how the boundary between “suitable design for polymer AM” and “suitable design for SBAM” can be determined in the context of part collapse under dead load. The investigations consist of a preliminary study and a main study.

Preliminary study

The following sections describe the preliminary study. In this study, different types of specimens are to be used to investigate whether the dead load induced stresses are the driver behind part failure. Failure mechanisms are analyzed to derive conclusions about the strength hypothesis applicable. In addition, the aim is to systematically approach the critical stress value for part design. The methodology, the experimental set-up and the results of the preliminary study are discussed.

Methodology

Determining material properties such as tensile strength is already a challenge for green parts. The most fragile state of the part is in the brown state, when all binders have been removed from the part. This state is reached directly before the sintering process is initialized. At this point, imperfections from the real test setup can significantly falsify the results of material testing. For this reason, specimens are manufactured for which the structural-mechanical properties and the resulting stresses are adjusted.

Two types of specimens are designed. The specimens have cylindrical cantilevers that protrude at either a 45° angle (see figure 3 (a)) or 0° angle (see figure 3 (b)) with respect to the build platform. The occurring stresses are systematically controlled by varying the diameter and length of the cylinders. The geometric configurations can be found in the appendix.

Figure 3: Exemplary CAD-designs of specimens for the preliminary study for (a) 45° angle and (b) 0° angle

Experimental set-up

The investigations are of a phenomenological character, thus physical specimens are manufactured and evaluated. Ti-6Al-4V feedstock (*Element22 GmbH*, Kiel, Germany and *Headmade Materials GmbH*, Unterpleichfeld, Germany), which is a near Grade 5 PM-Titanium alloy defined in the standard [20], is used as the material for the investigations. The material's chemical composition can be found in table 1. The feedstock is made from fine Ti-6Al-4V powder, which is coated with a polymer-based binder system. The size range of the powder agglomerates is between 50 and 200 microns. The CMF specimens are manufactured using a FORMIGA P110 (*EOS GmbH*, Krailing, Germany). The feedstock is processed at a layer height of 0.1 mm. Countours are manufactured with a scanning speed of 2000 mm/s and a laser power of 20 W. Hatches are manufactured with a scanning speed of 3500 mm/s and a laser power of 17 W. After printing, the specimens are chemically debound in an acetone bath at 50 °C for several hours. In the final process step, the specimens are thermally debound (between 150 - 400 °C) and sintered in a vacuum furnace (*MUT Advanced Heating GmbH*, Jena, Germany). Sintering takes place above 1000 °C for proper microstructural development. The specimens are manufactured in two iterations respectively two build jobs.

Table 1: Chemical composition of feedstock after sintering

Alloying elements in percent by weight (%)						
Ti	**Al**	**V**	**O**	**Fe**	**C**	**N**
Balance	5.5 - 6.75	3.5 – 4.5	≤ 0.30	≤ 0.30	≤ 0.05	≤ 0.05

The microscope images displayed are taken with a digital microscope VHX-7000 (*KEYENCE DEUTSCHLAND GmbH*, Neu-Isenburg, Germany). Furthermore, finite element analyses (FEA) are carried out alongside the tests. The FEAs are conducted based on the CAD geometries of the test specimens within the commercial software ANSYS Mechanical (*ANSYS, Inc.*, Canonsburg, USA). All FE simulations are carried out with a linear-elastic material model for small deformations. The contact surface of the specimens is set as fixed in the boundary conditions. Gravity acts on the specimens. This simplified approach is only intended to describe which stresses initiate the flow of the material. It is not suitable for modeling the deformation behavior over the manufacturing process. Standard element size is 0.5 mm, with the mesh being refined by a factor of 2 based on convergence investigations at the locations with stress concentrations.

Results

A total of 22 specimens were manufactured within this preliminary study, resulting in 44 manufactured cylinders. A share of the specimens has gone through the manufacturing process undamaged, the other share exhibited fractured geometries. For this scenario (continuous independent variables and dichotomous dependent variables), a logistic regression can be performed [21]. The results of the regression can be used to model the system behavior and evaluate the significance of the independent variables considered. The evaluation of the significance after creating the model using the analysis of variance method (ANOVA) shows that the maximum v. Mises stress as well as the maximum principal normal stress are significant, whether they are considered simultaneously in the model or individually. This makes sense, as both stress variables correlate strongly (correlation coefficient: 0.98). However, this does not indicate which stress variable is responsible for the part collapse. The fractures on the collapsed parts are examined for further analysis. An example of such a fracture is shown in figure 4.

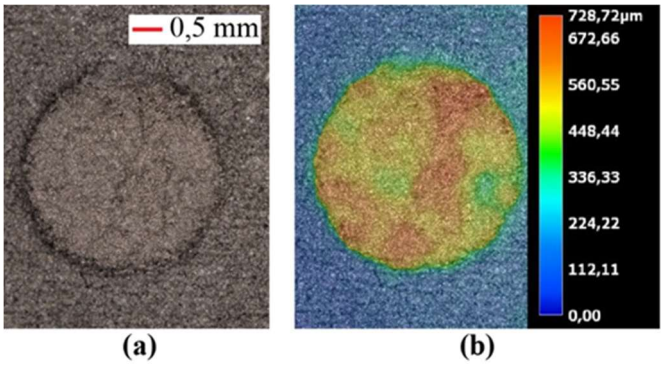

Figure 4: (a) Microscope image of fracture; (b) elevation profile of fracture

The fracture has no directional characteristics and the fracture strain is small. Both aspects indicate a brittle fracture. As described above, a part is most fragile when there is no binder at all. The cohesion within the component is only given by diffusion processes that have been initiated [3]. Part failure without external influence is most likely at this stage. The material structure on the fracture surface is the same as on the regular outer surfaces of the specimens. The spherical structure of the metal powder particles as well as attached sinter necks are distinguishable in both cases. This also indicates that the sintering occurred after the fracture. In addition, the final deformations of the fractured specimens indicate that the component fractured first and then shrinkage occurred. This is consistent with the assumption of fracture in the brown state, as significant part shrinkage only occurs during the subsequent diffusion processes during sintering [22]. Furthermore the assumption of brittle material behavior is emphasized by existing studies in the context of SBAM [23]. These observations lead to the assumption that quasi-brittle material behavior is given. According to [24], the principal stress hypothesis is to be applied for such materials, therefore in the main study the maximum principal stress is examined exclusively as a critical target value. The range for the critical stress value for the preliminary study is 22.3 kPa < $\sigma_{crit,CMF,pre} \leq$ 22.7 kPa.

Main study

The following sections describe the main study. Within this study, the methodology and findings of the preliminary study are applied to other feedstock systems and technologies. The methodology, the experimental set-up and the results of the preliminary study are discussed.

Methodology

In the main study, the findings and methodology from the preliminary study are transferred to two applications:

a. CMF with a different feedstock configuration compared to the preliminary study. This is a variation of the feedstock used in the preliminary study. The composition is unchanged, the difference lies in the coating process. Due to the changes in the coating process, the variance in both green part density and elongation at break in the sintered state could be reduced. The aim of this main study is to examine whether the modified coating process also has an effect on the stresses that can be handled during debinding and sintering.
b. Metal FFF with filament as feedstock. The aim is to investigate the extent to which the failure mode of CMF parts also applies to MFFF parts. It is assumed that there are critical stress limits as well. These limits are to be approached for various build directions.

The specimens from the preliminary study are further developed for this purpose. The specimens for CMF are designed to allow the same insights with less material consumption. For the MFFF process, the same geometries are manufactured in three different build directions to analyze the anisotropic layer effect before debinding and sintering and to identify influences on stress limits. This results in three different set-ups for the investigations on MFFF, which are shown in figure 5.

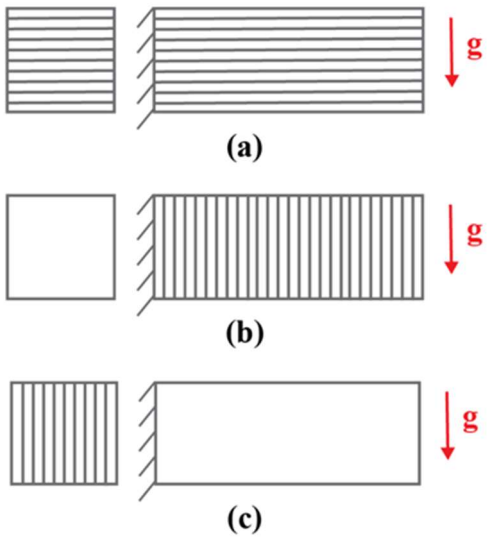

Figure 5: Layer orientation with respect to gravity of (a) set-up 1, (b) set-up 2 and (c) set-up 3

Figure 6 shows the respective cantilevers of the three different set-ups including the orientation of the layers. The lines are only used to represent the layers, the infill pattern within a layer is not shown. For the MFFF-process, no cylindrical geometries are

manufactured, but cuboid cantilevers. This enables printing without support structures in different orientations. The specimen design for CMF is shown in figure 6 (a). The lengths of the cantilevers on the CMF specimen and thus the induced stresses are derived from the findings of the preliminary study. The length of the 8 cantilevers is successively reduced from 24.5 mm to 19.25 mm respectively from 22.0 mm to 16.75 mm (tests are carried out in two iterations). This results in a stress range of 21.6 kPa to 10.0 kPa in the green state. Figure 6 (b) shows the specimen variant for MFFF set-up 1, (c) for set-up 2 and (d) for set-up 3. The different designs of the MFFF-specimens result from the build direction and the circumstance that support-free printing is desired. The lengths of the cantilevers are the same for set-up 1 and 2. The length decreases successively by 3 mm except for the shortest cantilever, which is 9 mm shorter than the nearest larger cantilever. The reason for this drop is that there is not yet enough experience for the critical stress value for the MFFF concerning different build directions. Thus, a possible low critical stress value should still be approximated. The lengths of the cantilevers for set-up 3 follow the same systematic approach but have different values than in the previous set-ups. This is due to the fact that the cantilevers for this set-up are attached differently to the basic geometry of the specimen and therefore different stresses are given. Stresses are the determining factor in these investigations. The complete experimental design can be found in the appendix.

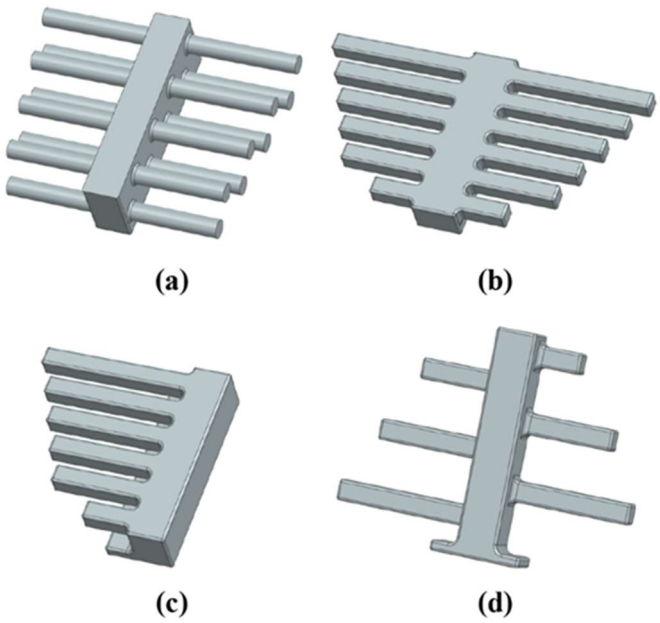

Figure 6: CAD-Geometries of (a) CMF-specimen and MFFF-specimen for (b) set-up 1, (c) set-up 2 and (d) set-up 3

Experimental set-up

The experimental set-up for the CMF process is the same as in the preliminary study besides the different version of the Ti-6Al-V4 feedstock (*Element22 GmbH*, Kiel, Germany and *Headmade Materials GmbH*, Unterpleichfeld, Germany). The specimens are manufactured in two iterations respectively two build jobs.

The MFFF specimens are printed on a FL300M (*FuseLab*, Peer, Belgium) utilizing a Ti-6Al-4V feedstock (*Element22 GmbH*, Kiel, Germany) in filament form. Layer height for this process is 0.1 mm as well with a printing speed of 40 mm/s and a nozzle temperature of 135 °C.

After printing, all specimens are chemically debound in an acetone bath at 50°C for several hours. In the final process step, the specimens are thermally debound (between 150 - 400 °C) and sintered in a vacuum furnace (*MUT Advanced Heating GmbH*, Jena, Germany). Sintering takes place above 1000 °C for proper microstructural development.

FEAs are carried out following the same set-up as in the preliminary study.

Results

The geometries produced via CMF show the same failure behavior as in the preliminary study. The cantilevers are not subject to any significant deformation and the fractures are of a brittle characteristic (see figure 7). Compared to the preliminary study, however, the range for the critical stress value is different: 14.0 kPa < $\sigma_{crit,CMF,main} \leq$ 14.3 kPa instead of 22.3 kPa < $\sigma_{crit,CMF,pre} \leq$ 22.7 kPa.

Depending on the build direction, a significantly different critical stress value appears to apply to the MFFF specimens. Figure 8 shows one specimen for each set-up after sintering. The specimens were sintered in the orientations shown. The specimens of set-up 1 were sintered on pedestals to ensure that the cantilevers would securely break. The determined critical stress values for set-up 1 are 13.7 kPa < $\sigma_{crit,MFFF,1} \leq$ 17.9 kPa, for set-up 2 2.7 kPa < $\sigma_{crit,MFFF,2} \leq$ 8.1 kPa and for set-up 3 17.9 kPa < $\sigma_{crit,MFFF,3} \leq$ 22.5 kPa.

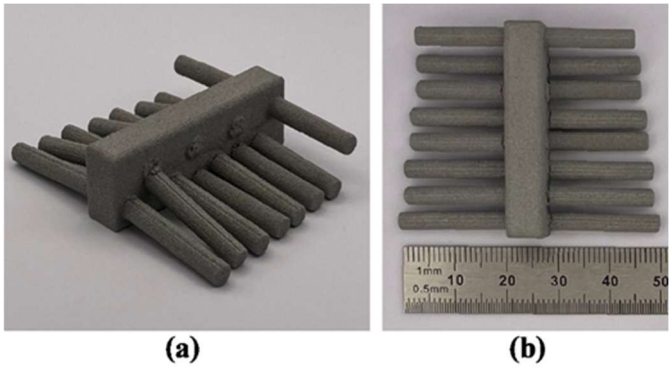

Figure 7: Physical CMF-specimen after sintering (a) perspective and (b) from above with scale

It is furthermore apparent that the brittle fracture behavior is similar to that of the CMF only for set-up 2. The cantilevers of this set-up are only slightly deformed and the broken cantilevers are all completely broken off (see figure 8). For set-up 1 and set-up 2, the geometries are subject to significantly larger deformations. Most of the fractured cantilevers only have cracks and no complete fractures. This applies in particular to long cantilevers. One explanation is that the possibilities for deflection in the direction of gravity are limited due to the orientation during debinding and sintering (see figure 9). As a result, a state of equilibrium between stresses and strains appears to be reached earlier for the long cantilevers than for the shorter cantilevers. For six of the 20 cantilevers manufactured with the longest or second longest length within set-up 1, this is even the case before cracking occurs.

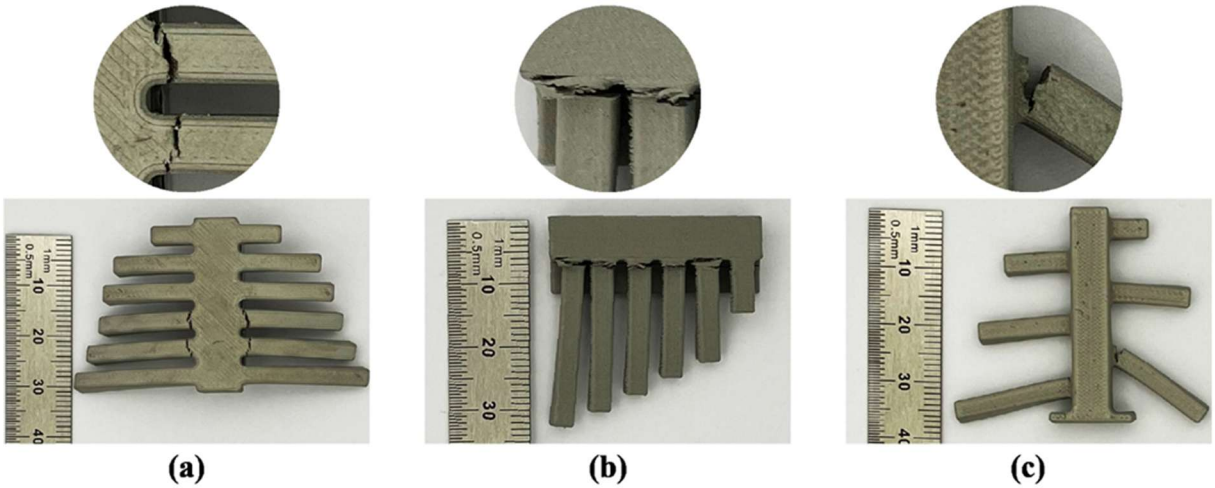

Figure 8: Respective sintered specimen with detail of fracture for (a) set-up 1, (b) set-up 2 and (c) set-up 3

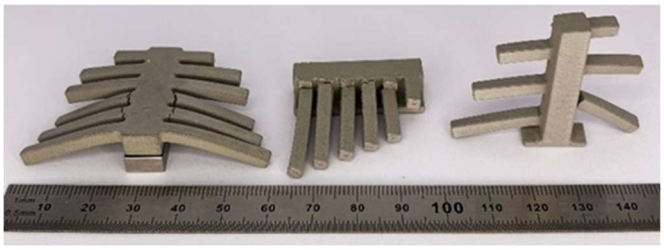

Figure 9: Sintered physical MFFF-specimens for set-up 1, 2 and 3 (left to right)

Case study

A so-called swan neck is optimized and manufactured via CMF for the case study. This part is a bracket of a racing car that is exposed to mechanical loads by holding the rear wing. This component possesses packing dimensions of approximately 18 mm x 60 mm x 63 mm and no strict tolerance requirements, which makes it ideally suited for manufacturing using sintering technologies. For the optimization of the part the software MSC Apex Generative Design (*Hexagon AB*, Stockholm, Sweden) is used. The software works on a stress-based algorithm. Therefore, the maximum achievable stress values are implemented within the respective load cases. The Ti-6Al-4V feedstock from the preliminary study is used for the case study. The optimization is carried out in two versions. In one version, the stress limit for debinding and sintering is not considered, in the other version it is.

The part is optimized for a total of five load cases. Four of these load cases result from part application. The fifth load case represents the load during debinding and sintering. Here, the bearing surface of the part is implemented as a fixture. Gravity is applied as load (see figure 10). For the load cases related to the part application, the tensile strength of sintered Ti-6Al-4V with a safety factor of two is used as the stress limit. For the debinding and sintering load case, a value of 15 kPa is defined as the stress target. It is important to note that the stress limits determined for the green part density are not utilized for the optimization. The FE simulations have shown that the gravity-induced stresses are directly proportional to the density of the parts. Since the optimization software works with the density of the sintered material, the critical stress value of the feedstock is adjusted to the density of this material:

$$\frac{\sigma_{crit,green}}{\rho_{green}} = \frac{\sigma_{crit,sintered}}{\rho_{sintered}}, \quad (1)$$

$$\rightarrow \sigma_{crit,sintered} = \rho_{sintered} \cdot \frac{\sigma_{crit,green}}{\rho_{green}}, \quad (2)$$

with $\rho_{sintered}$ = 4.42 g/cc and ρ_{green} = 3.12 g/cc.

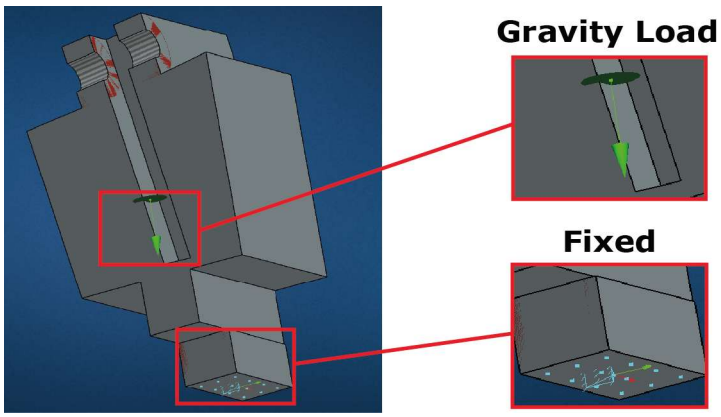

Figure 10: Debinding and sintering load case implemented within MSC Apex Generative Design

Figure 11 shows the CAD models of the two optimized part versions. The parts vary in detail, especially the upper section with the hollow cylinders for inserting the bolts in the later application is attached differently to the rest of the part depending on the optimization set-up. This attachment is the most critical location in the context of the dead load during debinding and sintering. This is shown by the FEA performed on the optimized parts. The settings for the FEA are the same as in the studies above. For the part without taking the debinding load case into account, the maximum value for the principal stress is 24.1 kPa (respectively 17.0 kPa in green state). For the other part, this value is 88.1 kPa (respectively 62.0 kPa in green state).

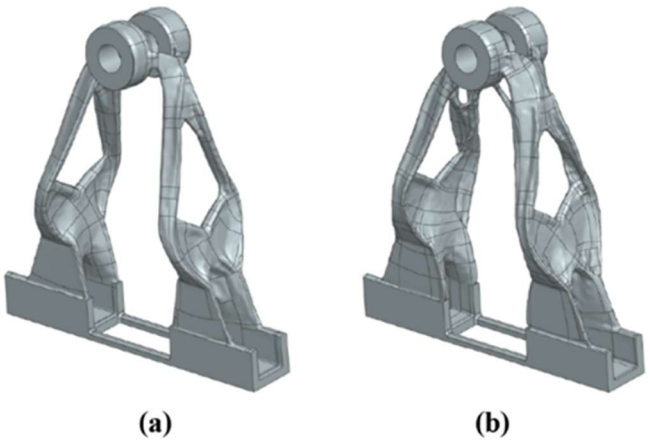

Figure 11: CAD-Designs of optimized mountings: (a) no debinding load case taken into account and (b) debinding load case taken into account

Both versions are manufactured four times each via CMF. Depowdering the fragile green parts directly after printing is particularly challenging, as the parts possess features with wall thicknesses of less than 1 mm and struts with a diameter of less than 1 mm due to the optimization. While all parts undergo chemical debinding undamaged, only the version optimized for the debinding load case passes through thermal debinding and sintering without failure. All four parts of this version are intact, while all four parts of the other version are destroyed. Figure 12 shows two parts (one of each version) after sintering.

Figure 12: Physical optimized parts after sintering

Conclusion and outlook

A total of 278 cantilevers were manufactured (of which 164 via CMF and 114 via MFFF). For CMF manufacturing process, the critical stress limits were determined for two Ti-6Al-4V feedstock systems in the context of the dead weight. For MFFF, a critical stress range was determined for a Ti-6Al-4V feedstock system for three different build orientations. The assumption that material behavior is quasi-brittle and that parts experience only small deformation before collapsing under their own dead load applies to CMF. This behavior also applies to the fracture behavior of MFFF parts where the dead load causes normal stresses in build direction (set-up 2). If the normal stresses caused by dead load are oriented normal to build direction, structures can withstand greater deformation before brittle fracture occurs (set-up 1 and 3). Table 2 contains the maximum stress values determined. The stress limits in connection with the dead load are listed both with respect to the green part density ($\sigma_{max,green}$) and with respect to the density as sintered ($\sigma_{max,sintered}$). If the respective stress value was adhered to, 100 % of the geometries could be Manufactured intact.

Table 2: Determined stress limits for examined technologies

Principal stress limits (kPa)	CMF		MFFF		
	Preliminary study	Main study	Set-up 1	Set-up 2	Set-up 3
$\sigma_{\text{principal,max,green}}$	22.3	14.0	13.7	2.7	17.9
$\sigma_{\text{principal,max,sintered}}$	31.7	19.9	19.5	3.8	25.5

The findings on the material behavior during debinding and sintering enable the evaluation of manufacturability of parts in the design phase. The worst case within these processing steps, part collapse under fracture, can thus be identified.

The findings were successfully applied in another context: automated part design. It was shown that the consideration of the identified critical stress value for debinding and sintering can be used as a load case in topology optimization. A stress-based algorithm was used for this purpose. By implementing this load case, a part was not only optimized for its application, but also with regard to its sinterability. This holds potential not only for manufacturing under “First Time Right”, but also for the entire product design process for SBAM parts.

As discussed in chapter 3, compliance with the stress limit is not a sufficient, but a mandatory prerequisite for the successful design for SBAM. The dimensional accuracy of the components after sintering depends on both the technology and the component design. As described in chapter 6, there are no strict requirements for tolerances of the part from the case study. If the bores in the component are to have a fit or if there are strict requirements regarding the position or shape of features, a corresponding material allowance must be used during machining. In this case, tolerance class IT12 according to [25] should be used as a reference for the allowance for this part. Components manufactured via CMF experience less deformation before collapsing than those manufactured via MFFF. Thus, for parts manufactured with the MFFF process, it must be taken into account that larger deformations can occur even though the critical stress limit is not exceeded. There are several ways to deal with this. On the one hand MFFF components potentially can be designed to compensate for deformation during debinding and sintering, allowing manufacturing without support structures. Approaches for this are examined in [5,6]. On the other hand, parts can be designed in such a way that they are as robust as possible against undesired deformations. A possible approach for this is discussed in [26].

There are aspects that have not yet been answered by the studies discussed. The first aspect is the potential for improvement of the simplistic FEA set-up. The approach utilized appears to be sufficient for the assessment of quasi-brittle material behavior where no large deformations occur prior to fracture. The applicability of this approach for scenarios in which relatively large deformations occur during debinding and sintering, as in MFFF set-up 1 and 3, is questionable. The approach used provides information on whether there is an impulse for such deformations due to the dead load. Depending on the part geometry, the resulting deformations can lead to altered stresses. These stresses cannot be considered by the applied approach. On the one hand, potentially different failure mechanisms apply to such material behavior. On the other hand, the set-up for the FEA would have to be different. Furthermore, the assumption of linear material behavior with small deformations cannot be used for such a scenario.

Further material parameters are also necessary if the aim is to describe material flow behavior. Such a set-up tends towards a transient process simulation. There are commercial products for this type of software. However, the primary focus of this software is on describing deformation behavior without fracture.

The material properties of deformed MFFF parts after sintering are another unresolved aspect. So far, it has not been investigated how deformations affect, for instance, the

relative density or the strength of the final part. Such insights are important in order to be able to assess potential risks for the use of deformed MFFF parts. This is also an important point with regard to the use of deformation compensation in part design.

An additional aspect is the reliability of the critical stress values determined. In the studies concerning CMF, it can be seen that the critical stress value is subject to deviations that appear to be related to the build job, among other things. The methodology for determining such critical stress values has been established and initial investigations have taken place. However, a statistically reliable conclusion regarding the critical stress value can neither be made for the CMF process nor for the MFFF process.

Acknowledgement

The project “Development of sinter-based generative process routes for aluminum and titanium alloys for topology-optimized lightweight components for the mobility sector (SIGNAL)” is funded by the Federal Ministry for Economic Affairs and Climate Action (BMWK, German Federal Ministry) in the Lightweight Technology Technology Transfer Program (TTP LB) under the funding code 03LB2060 and supervised by Project Management Jülich (PtJ).

Contributions

Conceptualization, D.S.; methodology, D.S.; validation, D.S. and T.M.; investigation, D.S.; writing - original draft preparation, D.S.; writing - review and editing, D.S., J.T. and T.M.; supervision, J.T.; funding acquisition, J.T.

All authors have read and agreed to the published version of the manuscript.

Appendix

Specimen geometries pre-sintering – Preliminary study

Geometry	Dimensions of cantilevers (mm) (⌀, length)
Cylindrical 45° angle	(5.0, 24.0); (5.0, 26.0); (5.0, 28.0); (5.0, 32.0); (5.0, 34.0)
Cylindrical 0° angle	(8.6, 22.0); (8.3, 24.5); (4.3, 23.8); (9.8, 28.5); (8.3, 27.9); (3.8, 23.6)

Specimen geometries pre-sintering – Main study

Study	Geometry and dimensions of cross section (mm)	Cantilevers' lengths (mm)
CMF	Cylindrical ⌀ = 4.0	19.25; 20.00; 20.75; 21.50; 22.25; 23.00; 23.75; 24.50 16.75; 17.50; 18.25; 19.00; 19.75; 20.50; 21.25; 22.00
FFF Set-up 1	Cuboid width = 4.0 height = 4.0	10.0; 19.0; 22.0; 25.0; 28.0; 31.0
FFF Set-up 2		8.5; 14.5; 17.5; 20.5; 23.5; 26.5
FFF Set-up 3		10.0; 19.0; 22.0; 25.0; 28.0; 31.0

Categorical Results

Study	$\sigma_{principal,max,green}$ (kPa)	$\sigma_{principal,max,sintered}$ (kPa)	# of manufactured cantilevers	# of cantilevers w/o fracture	% of cantilevers w/o fracture
CMF Pre Study	$\sigma \leq 22.3$	$\sigma \leq 31.7$	24	24	100 %
	$22.7 \leq \sigma \leq 26.8$	$32.3 \leq \sigma \leq 38.0$	16	12	75 %
	$29.2 \leq \sigma$	$41.4 \leq \sigma$	12	0	0 %
CMF Main Study	$\sigma \leq 14.0$	$\sigma \leq 19.9$	38	38	100 %
	$14.3 \leq \sigma \leq 16.7$	$20.3 \leq \sigma \leq 23.7$	42	11	26 %
	$17.2 \leq \sigma$	$24.4 \leq \sigma$	32	0	0 %
FFF Set-up 1	$\sigma \leq 13.7$	$\sigma \leq 19.5$	30	30	100 %
	$17.9 \leq \sigma$	$25.5 \leq \sigma$	30	4	13 %
FFF Set-up 2	$\sigma \leq 2.7$	$\sigma \leq 3.8$	5	5	100 %
	$8.1 \leq \sigma$	$11.5 \leq \sigma$	25	0	0 %
FFF Set-up 3	$\sigma \leq 17.9$	$\sigma \leq 25.5$	16	16	100 %
	$22.5 \leq \sigma$	$32.0 \leq \sigma$	8	8	0 %

References

[1] ISO/ASTM, "52900:2021 Additive Manufacturing – General principles – Fundamentals and vocabulary", ISO International Organization for Standardization, 2021

[2] M. Rupp et al., "Additive Manufacturing in the Scope of Industry 4.0: A Review on Energy Consumption and Building Time Estimation for Laser Powder Bed-Fusion Processes", Industry 4.0, 7(4), 118-122, 2022

[3] W. Schatt et al., "Pulvermetallurgie: Technologien und Werkstoffe", Springer-Verlag Berlin Heidelberg, 2007

[4] AMPOWER GmbH, "Metal Binder Jetting Implementation", AMPOWER Insights, 14, 2024

[5] M. Zago, N. F. M. Lecis, M. Vedani, I. Cristofolini, "Geometrical Issues in Design for Binder Jetting – The Effect of Anisotropic Dimensional Change on Sintering", Design Tools and Methods in Industrial Engineering II, Edited by C. Rizzi et al., Springer International Publishing, 2022

[6] I. Cristofolini, O. Uçak, M. Zago, B. Vicenzi, M. Dougan, M. Schneider, P. Pedersen, J. Voglhuber, "Design for sintering – A comprehensive study on anisotropic dimensional change on sintering", Powder Metallurgy, 67, 1-19, 2024

[7] D. Kaschube, T. Pawlowitz, C.-H. Solterbeck, J. Schloesser, M. Malekan, B. Bohlmann, "Fatigue behavior of Ti-6Al-4 V alloy manufactured by cold metal fusion", Fatigue & Fracture of Engineering Materials & Structures, 47, 2023

[8] M. Munsch, "Reduzierung von Eigenspannungen und Verzug in der laseradditiven Fertigung", Schriftenreihe Lasertechnik, 1, Cuvillier Verlag, 2013

[9] F. Shen, W. Zhu, K. Zhou, L.-L. Ke, "Modeling the temperature, crystallization, and residual stress for selective laser sintering of polymeric powder", Acta Mech, 232, 3635-3653, 2021

[10] Y. Thompson, "Additive Manufacturing by Metal Fused Filament Fabrication", FAU Studien Materialwissenschaft und Werkstofftechnik Band 26, FAU University Press, 2023

[11] C. Klahn et al., "Design Guidelines", Springer Handbook of Additive Manufacturing, Edited by E. Pei et al., Springer Nature Switzerland, 2023

[12] H. Blunk, A. Seibel, "Toward a Design Compendium for Metal Binder Jetting", Innovative Product Development by Additive Manufacturing 2021, Edited by R. Lachmayer et al., Springer International Publishing, 2023

[13] AMPOWER GmbH, "Design Guideline for sinter-based Additive Manufacturing", AMPOWER Insights, 8, 2022

[14] H. Blunk et al, "Design guidelines for metal binder jetting", Progress in Additive Manufacturing, 9(4), 2024

[15] G. A. O. Adam, “Systematische Erarbeitung von Konstruktionsregeln für die additiven Fertigungsverfahren Lasersintern, Laserschmelzen und Fused Deposition Modeling“, Forschungsberichte des Direct Manufacturing Research Centers, 1, Shaker Verlag, 2015

[16] J. Kranz, D. Herzog, C. Emmelmann, “Design guidelines for laser additive manufacturing of lightweight structures in TiAl6V4”, J. Laser Appl., 27(1), 2015

[17] Th. Reiher, “Intelligente Optimierung von Produktgeometrien für die additive Fertigung“, Forschungsberichte des Direct Manufacturing Research Centers, 12, Shaker Verlag, 2019

[18] D. Godec, S. Cano, C. Holzer, J. Gonzalez-Gutierrez, “Optimization of the 3D Printing Parameters for Tensile Properties of Specimens Produced by Fused Filament Fabrication of 17-4PH Stainless Steel”, Materials, 13(3):774, 2020

[19] A. Mostafaei, A. Elliott, J. Barnes, C. Cramer, P. Nandwana, M. Chmielus, “Binder jet 3D printing – process parameters, materials, properties, and challenges”, Progress in Materials Science, 100684, 2020

[20] ASTM International, “B988-18R22 Standard Specification for Powder Metallurgy (PM) Titanium and Titanium Alloy Structural Components“, 2022

[21] J. Hedderich, L. Sachs, “Angewandte Statistik – Methodensammlung mit R”, Springer Verlag Berlin Heidelberg, 2020

[22] S. Banerjee, C. J. Joens, “Debinding and sintering of metal injection molding (MIM) components”, Handbook of Metal Injection Molding, Edited by D. F. Heaney, Woodhead Publishing, 2012

[23] J. Gonzalez-Gutierrez, S. Cano, S. Schuschnigg, C. Kukla, J. Sapkota, C. Holzer, “Additive Manufacturing of Metallic and Ceramic Components by the Material Extrusion of Highly-Filled Polymers: A Review and Future Perspectives”, Materials, 11(5):840, 2018

[24] D. Gross, Th. Seelig, Bruchmechanik: Mit einer Einführung in die Mikromechanik, Springer Vieweg Berlin Heidelberg, 2016

[25] DIN-Normenausschuss Technische Grundlagen, “DIN EN ISO 286-1 Geometrical product specifications (GPS) - ISO code system for tolerances on linear sizes - Part 1: Basis of tolerances, deviations and fits”, Deutsches Institut für Normung, 2019

[26] D. Stachg, T. Marter, J. Telgkamp, “Ways to robust Part Designs for Additively Manufactured Sinter Parts through Lightweight Design Techniques”, Materials Science and Engineering Congress, Darmstadt, 2024

Contact details

David Stachg (Corresponding author)
Berliner Tor 21, 20099 Hamburg
E-Mail: david.stachg@haw-hamburg.de